

X-ray, Optical, and Radio Observations of SN 1999em and SN 1998S

David Pooley¹, Walter H. G. Lewin¹, Derek W. Fox^{1,2}, Jon M. Miller¹, Christina K. Lacey³, Schuyler D. Van Dyk⁴, Kurt W. Weiler⁵, Richard A. Sramek⁶ Alexei V. Filippenko⁷, Douglas C. Leonard⁷, Stefan Immler⁸, Roger A. Chevalier⁹, Andrew C. Fabian¹⁰, Claes Fransson¹¹, Ken'ichi Nomoto¹²

ABSTRACT

Observations of the Type II-P (plateau) Supernova (SN) 1999em and Type IIn (narrow emission line) SN 1998S have enabled estimation of the profile of the SN ejecta, the structure of the circumstellar medium (CSM) established by the pre-SN stellar wind, and the nature of the shock interaction. SN 1999em is the first and only Type II-P detected at both X-ray and radio wavelengths. It is the least radio luminous and one of the least X-ray luminous SN ever detected (except for the unusual and very close SN 1987A). The *Chandra* X-ray data indicate non-radiative interaction of SN ejecta with a power-law density profile ($\rho \propto r^{-n}$ with $n \sim 7$) with a pre-SN wind with a low mass loss rate of $\sim 2 \times 10^{-6} M_{\odot} \text{ yr}^{-1}$ for a wind velocity of 10 km s^{-1} , in close agreement with radio mass-loss rate estimates. The *Chandra* data show an unexpected, temporary rise in the 0.4–2.0 keV X-ray flux at ~ 100 days after explosion. SN 1998S appears reasonably typical of Type IIn SNe in that it is developing very slowly. At an

¹Center for Space Research and Department of Physics, Massachusetts Institute of Technology, Cambridge, MA 02139-4307; dave@mit.edu, lewin@space.mit.edu, derekfox@space.mit.edu, jmm@space.mit.edu

²Current Address: Astronomy Department, California Institute of Technology, Mail Code 105-24, Pasadena, CA 91125

³Department of Physics and Astronomy, University of South Carolina, Columbia, SC 29208; lacey@sc.edu

⁴Infrared Processing and Analysis Center, California Institute of Technology, Mail Code 100-22, Pasadena, CA 91125; vandyk@ipac.caltech.edu

⁵Naval Research Laboratory, Code 7213, Washington DC 20375-5320; weiler@rsd.nrl.navy.mil

⁶National Radio Astronomy Observatory, Socorro, NM 87801; dsramek@nrao.edu

⁷Department of Astronomy, University of California, Berkeley, CA 94720-3411; alex@astron.berkeley.edu, leonard@astron.berkeley.edu

⁸Astronomy Department, University of Massachusetts, Amherst, MA 01003; immler@astro.umass.edu

⁹Department of Astronomy, University of Virginia, Charlottesville, VA 22903; rac5x@virginia.edu

¹⁰Institute of Astronomy, Madingley Road, Cambridge, CB3 OHA, England, UK; acf@ast.cam.ac.uk

¹¹Stockholm Observatory, SE-133 36 Saltsjöbaden, Sweden; claes@astro.su.se

¹²Department of Astronomy and Research Center for the Early Universe, School of Science, University of Tokyo, Bunkyo-ku, Tokyo 113-0033, Tokyo, Japan; nomoto@astron.s.u-tokyo.ac.jp

age of >3 years, it is still bright in X-rays and is increasing in flux density at cm radio wavelengths. Spectral fits to the *Chandra* data indicate that a possible overabundance of Fe with respect to solar values is needed to account for the observed Fe line near 6.8 keV. If the X-ray emission is from the reverse shock wave region, the supernova density profile must be moderately flat at a velocity $\sim 10^4$ km s $^{-1}$, the shock front is non-radiative at the time of the observations, and the mass-loss rate is $1-2 \times 10^{-4}$ M $_{\odot}$ yr $^{-1}$ for a pre-supernova wind velocity of 10 km s $^{-1}$. This result is also supported by modeling of the radio emission which implies that SN 1998S is surrounded by a clumpy or filamentary CSM established by a high mass-loss rate, $\sim 2 \times 10^{-4}$ M $_{\odot}$ yr $^{-1}$, from the pre-supernova star.

Subject headings: supernovae: individual (SN 1998S, SN 1999em) — stars: mass loss — X-rays: individual (SN 1998S, SN 1999em) — X-rays: ISM — radio continuum: ISM

1. Introduction

To date, just 14 supernovae (SNe) have been detected in X-rays in the near aftermath (days to years) of their explosions¹³. In general, the high X-ray luminosities of these 14 SNe ($L_x \sim 10^{38}-10^{41}$ erg s $^{-1}$) dominate the total radiative output of the SNe starting at an age of about one year. This soft X-ray ($\lesssim 10$ keV) emission is most convincingly explained as thermal radiation from the “reverse shock” region that forms within the expanding SN ejecta as it interacts with the dense stellar wind of the progenitor star.

The interaction of a spherically symmetric SN shock and a smooth circumstellar medium (CSM) has been calculated in detail (Chevalier & Fransson 1994; Suzuki & Nomoto 1995). As the SN “outgoing” shock emerges from the star, its characteristic velocity is $\sim 10^4$ km s $^{-1}$, and the density distribution in the outer parts of the ejecta can be approximated by a power-law in radius, $\rho \propto r^{-n}$, with $7 \lesssim n \lesssim 20$. The outgoing shock propagates into a dense CSM formed by the pre-SN stellar wind. This wind is slow ($v_w \sim 10$ km s $^{-1}$) and has a high mass loss rate ($\dot{M} \sim 10^{-4}-10^{-6}$ M $_{\odot}$ yr $^{-1}$). The CSM density for such a wind decreases as the square of the radius ($\rho = \dot{M}/4\pi r^2 v_w$). The collision between the stellar ejecta and the CSM produces a “reverse” shock, which travels outward at $\sim 10^3$ km s $^{-1}$ slower than the fastest ejecta. Interaction between the outgoing shock and the CSM produces a very hot shell ($\sim 10^9$ K) while the reverse shock/ejecta interaction produces a denser, cooler shell ($\sim 10^7$ K) with much higher emission measure and is where most of the observable X-ray emission arises. If either the CSM density or n is high, the reverse shock is radiative, resulting in a dense, partly-absorbing shell between the two shocks.

Chevalier (1982) proposed that the outgoing shock from the SN explosion generates the relativistic electrons and enhanced magnetic field necessary for synchrotron radio emission. The

¹³A complete list of X-ray SNe and references can be found at <http://xray.astro.umass.edu/sne.html>.

ionized CSM absorbs most of this emission, except in cases where synchrotron self-absorption initially dominates, as may have been the case in SN 1993J (Chevalier 1998; Fransson & Björnsson 1998). However, as the shock passes rapidly outward through the CSM, progressively less ionized material is left between the shock and the observer, and absorption decreases rapidly. The observed radio flux density rises accordingly. At the same time, emission from the shock region is decreasing slowly as the shock expands so that, when radio absorption has become negligible, the radio light curve follows this decline. Observational evidence also exists at optical wavelengths for this interaction of SN shocks with the winds from pre-supernova mass loss (Filippenko 1997).

All known radio supernovae appear to share common properties of (i) non-thermal synchrotron emission with a high brightness temperature, (ii) a decrease in absorption with time, resulting in a smooth, rapid turn-on first at shorter wavelengths and later at longer wavelengths, (iii) a power-law decline of the emission flux density with time at each wavelength after maximum flux density (absorption $\tau \approx 1$) is reached at that wavelength, and, (iv) a final, asymptotic approach of the spectral index α to an optically thin, non-thermal, constant negative value (Weiler et al. 1986). These properties are consistent with the Chevalier model.

The signatures of circumstellar interaction in the radio, optical, and X-ray regimes have been found for a number of Type II SNe such as the Type II-L SN 1979C (Fesen & Matonick 1993; Immler et al. 1998; Weiler et al. 1986, 1991) and the Type II-L SN 1980K (Canizares et al. 1982; Fesen & Becker 1990; Leibundgut et al. 1991; Weiler et al. 1986, 1992). The Type IIn subclass has peculiar optical characteristics: narrow H α emission superposed on a broad base; lack of P Cygni absorption-line profiles; a strong blue continuum; and slow evolution (Schlegel 1990). The narrow optical lines are clear evidence for dense circumstellar gas — they probably arise from the reprocessing of the X-ray emission — and are another significant means by which the shock radiatively cools. The best recent examples of Type IIn SNe include SN 1978K, SN 1986J, SN 1988Z, SN 1994W (which may have been a peculiar Type II-P, Sollerman et al. 1998), SN 1995N, SN 1997eg, and SN 1998S.

SN 1999em was optically discovered on 1999 Oct 29 in NGC 1637, approximately 15'' west and 17'' south of the galactic nucleus (Li et al. 1999). The spectrum on 1999 Oct 29 shows a high temperature (Baron et al. 2000), indicating that the supernova was discovered at an early phase. We take 1999 Oct 28 as the date of the explosion. SN 1999em reached a peak brightness of $m_V \approx 13.8$ mag on about day 4, and remained in the “plateau phase,” an enduring period of nearly constant V-band brightness, until about 90 days after discovery (Leonard et al. 2001b). At an estimated distance of 7.8 Mpc (Sohn & Davidge 1998), this is the closest Type II-P supernova yet observed, and it is the only Type II-P observed in both X-rays and radio. Its maximum brightness of $M_V \approx -15.75$ marks it as one of the optically faintest SNe II-P (Patat et al. 1994).

On 1998 Mar 3, SN 1998S was optically discovered 16'' west and 46'' south of the nucleus of NGC 3877 (Li et al. 1998). Its spectrum quickly revealed it to be a peculiar Type IIn, with narrow H and He emission lines superimposed on a blue continuum (Filippenko & Moran 1998) along with strong N III, C II, C III, and C IV emission (Garnavich et al. 1998a; Liu et al. 2000) similar to the

“Wolf-Rayet” features seen in the early observations of SN 1983K (Niemela et al. 1985). SN 1998S reached a peak brightness of $m_V \approx 12$ (Granslo et al. 1998; Garnavich et al. 1998b). For a distance of 17 Mpc (Tully 1988), the intrinsic brightness of $M_V \approx -18.8$ marks SN 1998S as one of the optically brightest Type II SNe (Patat et al. 1993).

2. Observations

2.1. SN 1999em

2.1.1. X-ray

The trigger for our first *Chandra* observation was the optical discovery of a SN within 10 Mpc. The extremely rapid response of the *Chandra* staff allowed us to catch SN 1999em three days after discovery. We observed SN 1999em on 1999 Nov 1, Nov 13, Dec 16, 2000 Feb 7, and Oct 30 (days 4, 16, 49, 102, and 368 from reference). A summary of the observations is given in Table 1. All observations were performed by the Advanced CCD Imaging Spectrometer (ACIS) with the telescope aimpoint on the back-side illuminated S3 chip, which offers increased sensitivity to low energy X-rays over the front-side illuminated chips. The data were taken in timed-exposure (TE) mode using the standard integration time of 3.2 sec per frame and telemetered to the ground in very faint (VF) mode for the first two observations and faint (F) mode for the rest. In very faint mode, the telemetered data contain the values of 5×5 pixel islands centered on each event, while in faint mode the islands are 3×3 pixels.

2.1.2. Radio

We observed SN 1999em over 30 times with the VLA¹⁴ at frequencies ranging from 43.3 GHz to 1.5 GHz and ages from 3 to 454 days after the discovery date of 1999 Oct 29. Except for six weak but significant ($> 3\sigma$) detections at mid-cm wavelengths (1.5 – 8.4 GHz) at ages of between 33 and 69 days, all measurements yielded only upper limits.

2.1.3. Optical

We conducted extensive optical ground-based observations of SN 1999em; these include *UBVRI* photometry, long-term spectroscopy, and spectropolarimetry (Leonard et al. 2001a). These data will be used to derive a precise distance measurement with the Expanding Photosphere Method (Leonard et al. 2001b). Both the photometry and spectroscopy suggest that this was a relatively

¹⁴The VLA is operated by the NRAO of the AUI under a cooperative agreement with the NSF.

normal Type II-P event. We note, however, that SN 1999em was about 1 magnitude fainter than any of the 8 SNe II-P with EPM-derived distances and may have also had a slightly unusual color evolution (Leonard et al. 2001b).

Spectropolarimetry of SN 1999em was obtained on 1999 Nov 5, Dec 8, and Dec 17 (7, 40, and 49 days after discovery, respectively, while it was still in its plateau phase) with the Kast double spectrograph (Miller & Stone 1993) with polarimeter at the Cassegrain focus of the Shane 3-m telescope at Lick Observatory. Similarly, on 2000 Apr 5 and 9 (159 and 163 days after discovery, long after the plateau), we used the Low-Resolution Imaging Spectrometer (Oke et al. 1995) in polarimetry mode (LRISp; Cohen 1996) at the Cassegrain focus of the Keck-I 10-m telescope. Leonard et al. (2001a) discuss the details of the polarimetric observations and reductions.

Total flux spectra were obtained at many epochs, primarily with the Nickel 1-m and Shane 3-m reflectors at Lick Observatory. *UBVRI* photometry was conducted with the 0.8-m Katzman Automatic Imaging Telescope (KAIT) (Li et al. 2000; Filippenko et al. 2001) at Lick Observatory. These data and their implications will be thoroughly discussed by Leonard et al. (2001b).

2.2. SN 1998S

2.2.1. *X-ray*

Our criterion for *Chandra* observations of SNe beyond 10 Mpc was the detection of radio emission. SN 1998S was detected in the radio on 1999 Oct 28 (Van Dyk et al. 1999), and subsequent reanalysis of early radio observations indicated very weak detection at 8.46 GHz as early as 1999 Jan 07 (Lacey et al. 2001). We observed with *Chandra* on 2000 Jan 31, Mar 7, Aug 1, and 2001 Jan 14 (days 668, 725, 872, and 1038 since optical discovery). Similar to the observations of SN 1999em, these data were taken with the ACIS-S3 chip at nominal frame time (3.2 sec) in TE mode and telemetered in faint mode. A summary of the observations is listed in Table 2.

2.2.2. *Radio*

We observed SN 1998S over 20 times with the VLA at frequencies ranging from 22.48 GHz to 1.46 GHz and ages from 89 to 1059 days after the discovery date of 1998 Mar 03. All observations yielded only upper limits until 1999 Jan 07, age 310 days, when a weak detection was obtained. Since that time, monitoring has continued and SN 1998S has increased in flux density at all mid-cm wavelengths.

2.2.3. Optical

On 1998 Mar 7, just 5 days after the discovery of SN 1998S, we obtained optical spectropolarimetry of the supernova with LRISp on the Keck-II 10-m telescope. Total flux spectra were obtained over the first 494 days after discovery, as follows: (a) at Keck using LRIS on 1998 Mar 5, 6, and 27, and on 1999 Jan 6, and (b) at the Lick 3-m Shane reflector using the Kast double spectrograph on 1998 Jun 18, Jul 17 and 23, and Nov 25, and on 1999 Jan 10, Mar 12, and Jul 7. See Leonard et al. (2000) for details of the optical observations and reductions.

3. *Chandra* Data Reduction

For each observation, we followed the data preparation threads provided by the *Chandra* team and given on their website (http://asc.harvard.edu/ciao/documents_threads.html). We used the *Chandra* Interactive Analysis of Observations (CIAO) software to perform the reductions. We have used the most up-to-date (as of March 2001) set of calibration files (gain maps, quantum efficiency, quantum efficiency uniformity, effective area) available for each particular observation. Bad pixels were excluded, and intervals of bad aspect were eliminated.

All data were searched for intervals of background flaring, in which the count rate can increase by factors of up to 100 over the quiescent rate.¹⁵ The light curves of background regions were manually inspected to determine intervals in which the quiescent rate could be reliably calculated. In accordance with the prescription given by the ACIS Calibration Team, we identify flares as having a count rate $\gtrsim 30\%$ of the quiescent rate. Background flares were found in each of the first four observations of SN 1999em, lasting from hundreds of seconds to over 15 ksec. Only the second observation of SN 1998S had such a flare, lasting ~ 300 sec. The event lists were filtered to exclude the time intervals during which flares occurred. Effective observation times after filtering are listed in Tables 1 and 2.

In addition, we have performed a reprocessing of all data so as not to include the pixel randomization that is added during standard processing. This randomization has the effect of removing the artificial substructure (Moiré pattern) that results as a byproduct of spacecraft dither. Since all of our observations contained a substantial number of dither cycles (one dither cycle has a period of ~ 1000 sec), this substructure is effectively washed out, and there is no need to blur the image with pixel randomization. Removing this randomization slightly improves the point spread function (PSF).

The SNe spectra were extracted with the CIAO tool *dmextract*. We excluded events with a pulse invariant (PI) of either 0 (underflow bins) or 1024 (overflow bins). The region of extraction was determined from the CIAO tool *wavdetect*, a wavelet-based source detection algorithm which

¹⁵For a discussion of background flaring, see http://asc.harvard.edu/cal/Links/Acis/acis/Cal_prods/bkgrnd/current/index.html.

can characterize source location and extent. The data were restricted to the energy range of 0.4–8.0 keV for the purposes of spectral analysis since the effective area of ACIS falls off considerably below 0.4 keV and the increased background about 8 keV makes this data unreliable.

4. Results

4.1. SN 1999em

4.1.1. X-ray

The source was detected on all occasions, and an overlay of the X-ray contours from the first observation on an optical image of the host galaxy is shown in Fig. 1. The low flux ($F_x \lesssim 10^{-14}$ erg cm $^{-2}$ s $^{-1}$) resulted in few total counts (see Table 1). We have fit both the MEKAL and thermal Bremsstrahlung models to our data. The MEKAL model is a single-temperature, hot diffuse gas (Mewe et al. 1985) with elemental abundances set to the solar values of Anders & Grevesse (1989). We have calculated the column density (Predehl & Schmitt 1995) to be $N_H = 6.1 \times 10^{20}$ cm $^{-2}$ based upon a value of $E_{(B-V)} = 0.05$ (Baron et al. 2000). For both models, only the temperatures and overall normalizations were allowed to vary. In XSPEC (Arnaud 1996), we performed maximum likelihood fits on the unbinned data using Cash statistics (Cash 1979). These fits should be insensitive to the number of counts per channel and are thus appropriate for fitting low-count data. The results are shown in Table 3. As expected, the uncertainties in fit parameters for such low-count data are large.

We have also used flux ratios to characterize the source. The fluxes were calculated by manually integrating the source spectra, i.e., they are model-independent, absorbed fluxes. The first observation had a flux ratio of $F_x[2\text{--}8\text{ keV}]/F_x[0.4\text{--}2\text{ keV}] = 2.1 \pm 0.9$, but later observations were softer (Table 1). Somewhat surprisingly, the total flux nearly doubled from the third observation to the fourth, despite the continued decline of the high-energy X-rays. The multicolour X-ray lightcurve is shown in Fig. 2.

4.1.2. Radio

After 15 unsuccessful VLA observations of SN 1999em at ages 4 to 19 days after the assumed explosion date of 1999 Oct 28, the SN was finally detected on day 34 with 0.190 mJy flux density at 8.435 GHz. Subsequent observing on days 46, 60, and 70 indicated that SN 1999em remained detectable at a similar flux density, near the sensitivity limit of the VLA, at 8.435, 4.885, and 1.465 GHz. The data are shown, together with the x-ray results, in Fig. 2. Since day 70, no radio detection of SN 1999em in any cm wavelength band has been obtained. SN 1999em is the first and only radio detected Type II-P, so its behavior cannot be compared with other radio observations of the same type SN. An estimated spectral luminosity of SN 1999em at 6 cm peak on day ∼34 of

$L_{6\text{cm peak}} \sim 2.2 \times 10^{25} \text{ erg s}^{-1} \text{ Hz}^{-1}$ makes it the least radio luminous RSN known except for the peculiar, and very near, SN 1987A.

Under the Chevalier model of a dense CSM established by a slow pre-SN stellar wind ($v_w = 10 \text{ km s}^{-1}$, $v_{\text{shock}} = 10^4 \text{ km s}^{-1}$, $T = 2 \times 10^4 \text{ K}$; see, e.g., Weiler et al. 1986), such a radio luminosity is interpreted as indicative of a mass loss rate of $\sim 2 \times 10^{-6} \text{ M}_\odot \text{ yr}^{-1}$. The radio position of the emission from SN 1999em is RA(J2000) = $04^h 41^m 27.^s157$, Dec(J2000) = $-02^\circ 51'45.^''83$. The details of the observations and analysis can be found in Lacey et al. (2001).

4.1.3. Optical

Our spectropolarimetry of SN 1999em provides a rare opportunity to study the geometry of the electron-scattering atmosphere of a “normal” core-collapse event at multiple epochs. A very low but temporally increasing polarization level suggests a substantially spherical geometry at early times that becomes more aspherical at late times as ever-deeper layers of the ejecta are revealed. When modeled in terms of oblate, electron-scattering atmospheres, the observed polarization implies an asphericity of at least 7% during the period studied. We speculate that the thick hydrogen envelope intact at the time of explosion in SNe II-P might serve to dampen the effects of an intrinsically aspherical explosion. The increase in asphericity seen at later times is consistent with a trend recently identified (Wang et al. 2001) among stripped-envelope core-collapse SNe: the deeper we peer, the more evidence we find for asphericity. The natural conclusion that it is an *explosion* asymmetry that is responsible for the polarization has fueled the idea that some core-collapse SNe produce gamma-ray bursts (GRB; e.g., Bloom et al. 1999) through the action of a jet of material aimed fortuitously at the observer, the result of a “bipolar,” jet-induced, SN explosion (Khokhlov et al. 1999; Wheeler et al. 2000; Maeda et al. 2000).

4.2. SN 1998S

4.2.1. X-ray

The source was detected on all occasions, and an overlay of the X-ray contours from the first observation on an optical image of the host galaxy is shown in Fig. 3. In addition to constructing multicolour X-ray lightcurves (Fig. 4), the high luminosity of SN 1998S ($L_x \approx 10^{40} \text{ erg s}^{-1}$) allowed for basic spectral fitting to be done for each observation. We performed this in XSPEC with the VMEKAL model, which is similar to the MEKAL model but allows individual elemental abundances to vary. Using the reddening $E_{(B-V)} = 0.23$ (Leonard et al. 2000), we calculated the hydrogen column density to be $N_{\text{H}} = 1.36 \times 10^{21} \text{ cm}^{-2}$ (Predehl & Schmitt 1995). We used a redshift of $z = 0.003$ (Willick et al. 1997).

Although there were sufficient counts (>500 per observation) for spectral modeling, there were

few counts per energy channel. To mitigate the problems associated with fitting such data, we grouped the data to contain a minimum number of counts per bin. Because there were virtually no counts above ~ 7 keV in any of the observations, we would “smear” the Fe line at 6.7 keV if we required more than ~ 7 counts per bin. Therefore, we set the minimum number of counts per bin to the highest possible value which would still retain the integrity of the Fe line. This turned out to be 5 counts per bin for the first observation, 7 for the second, 5 for the third, and 7 for the fourth.

To reduce the number of free parameters in our fits, we froze the abundance of He to its solar value. We also linked the abundances of N, Na, Al, Ar, and Ca to vary with C. The remaining elemental abundances (O, Ne, Mg, Si, S, Fe, and Ni) were allowed to vary independently. We first allowed the column density to vary in our fits. Since the best-fit results were all consistent with the N_{H} obtained from the optical reddening, we fixed this parameter at the calculated value.

We then performed χ^2 fitting using Gehrels weighting for the statistical error (Gehrels 1986), which is appropriate for low count data. We also performed maximum likelihood fits to the unbinned data using Cash statistics (Cash 1979). The maximum likelihood fits were in good agreement with the χ^2 fits, and we report the χ^2 results here. For ease of viewing, we have plotted the best fit models against evenly binned data (Fig. 5).

We find the fits to be generally acceptable. They indicate that a possible overabundance of Fe (with respect to solar values) is needed to account for the observed Fe line near 6.8 keV. Averaging observations 2 and 4, we find that an overabundance is significant at $\sim 2.5 \sigma$. However, the data constrain neither the temperature nor the Fe abundance well (Table 4). The 2–10 keV luminosity decreases throughout all observations. Our spectral fitting model assumes collisional equilibrium. For the model described in Sec. 5.2, this is a valid assumption because of the high gas density.

To quantify the strength of the Fe line, we modelled it as a Gaussian on top of a power-law continuum. This model does not give formally acceptable fits to the entire data set, but does match the data well in the area of interest. We were interested in calculating the equivalent width of the feature, which we use to characterize its strength. The Fe line seems to have strengthened in the second observation but weakened in each subsequent observation (Table 5). The data do not constrain the line width well.

We also note that there is weak indication of an emission feature around 1.8 keV in the observations, similar to that seen in SN 1995N (Fox et al. 2000). We tested the significance of a Gaussian addition to the VMEKAL model. The F -statistic levels were 2.80%, 29.8%, 0.37%, and 2.10%, respectively, for the four observations. This represents the probability that the addition of the Gaussian component is unnecessary. For the marginally significant result of the third observation, the best fit line energy is $1.93_{-0.10}^{+0.10}$ (90% limits), which is (barely) consistent with fluorescent Si emission (Si K α and K β neutral line energies are 1.74 keV and 1.84 keV).

4.2.2. Radio

Since its initial radio detection at 8.46 GHz on 1999 Jan 07 (310 days after optical discovery), SN 1998S has increased at all mid-cm wavelengths. Modeling indicates that it should reach its 6 cm flux density peak at age \sim 1000 days, at roughly the epoch of the most recent observations on 2001 Jan 25. Assuming that is the case, SN 1998S is behaving like a fairly typical Type IIn (SN 1986J and SN 1988Z both peaked at 6 cm wavelength at age \sim 1000 days) although it will be the least radio luminous at 6 cm peak ($L_{6\text{cm peak}} \sim 3.6 \times 10^{26} \text{ erg s}^{-1} \text{ Hz}^{-1}$) of the six Type IIn RSNe known (SN 1978K, SN 1986J, SN 1988Z, SN 1995N, SN 1997eg, and SN 1998S). The radio data are shown together with the X-ray results in Fig. 4.

Under the Chevalier model of a dense CSM established by a slow pre-supernova stellar wind ($v_w = 10 \text{ km s}^{-1}$, $v_{\text{shock}} = 10^4 \text{ km s}^{-1}$, $T = 2 \times 10^4 \text{ K}$; see, e.g., Weiler et al. 1986), such a radio luminosity is interpreted as indicative of a mass loss rate of $\sim 2 \times 10^{-4} \text{ M}_\odot \text{ yr}^{-1}$. The radio position of the emission from SN 1998S is RA(J2000) = $11^h 46^m 06.^s140$, Dec(J2000) = $47^\circ 28'55.''45$. Although the details of the observations and analysis can be found in Lacey et al. (2001), it should be noted that the best fit to the radio data requires significant clumping or filamentation in the CSM, as was also found for the Type IIn SNe 1986J and 1988Z (Weiler et al. 1990; Van Dyk et al. 1993).

4.2.3. Optical

We found that SN 1998S exhibits a high degree of linear polarization, implying significant asphericity for its continuum-scattering environment (Leonard et al. 2000). Prior to removal of the interstellar polarization, the polarization spectrum is characterized by a flat continuum (at $p \approx 2\%$) with distinct changes in polarization associated with both the broad (symmetric, half width near zero intensity $\gtrsim 10,000 \text{ km s}^{-1}$) and narrow (unresolved, full width at half maximum $< 300 \text{ km s}^{-1}$) line emission seen in the total flux spectrum. When analyzed in terms of a polarized continuum with unpolarized broad-line recombination emission, an intrinsic continuum polarization of $p \approx 3\%$ results, suggesting a global asphericity of $\gtrsim 45\%$ from the oblate, electron-scattering dominated models of Höflich (1991). The smooth, blue continuum evident at early times is inconsistent with a reddened, single-temperature blackbody, instead having a color temperature that increases with decreasing wavelength. Broad emission-line profiles with distinct blue and red peaks are seen in the total flux spectra at later times, suggesting a disk-like or ring-like morphology for the dense ($n_e \approx 10^7 \text{ cm}^{-3}$) circumstellar medium, generically similar to what is seen directly in SN 1987A, although much denser and closer to the progenitor in SN 1998S. Such a disk/ring-like circumstellar medium may have formed from a merging of a binary-companion star that ejects the common-envelope material in the direction of the orbital plane of the binary system (Nomoto, Iwamoto, & Suzuki 1995).

5. Discussion

5.1. SN 1999em

To interpret the X-ray and radio data on SN 1999em, we use the circumstellar interaction model proposed by Chevalier (1982), and elaborated by Chevalier & Fransson (1994) and Fransson, Lundqvist, & Chevalier (1996; hereafter, FLC96). The outer supernova ejecta are taken to be freely expanding, with a power law density profile

$$\rho_{sn} = At^{-3}(r/t)^{-n}, \quad (1)$$

where A and n are constants. SN 1999em was a Type II-P supernova so we expect that the star exploded as a red supergiant with most of its hydrogen envelope. The value of n for such a star is usually taken to be in the range 7 – 12 (Chevalier 1982), although Matzner & McKee (1999) recently found that the explosion of a red supergiant leads to $n = 11.9$ at high velocity. In the case of SN 1999em, we have some additional information from modeling of the optical spectrum. Baron et al. (2000) were able to model spectra on 1999 Oct 29 and Nov 4/5 with $n = 7, 8$, or 9 . The modeling of the data for the earlier time suggests a relatively flat density profile ($n = 7$). The spectra on 1999 Oct 29 also show evidence for a secondary absorption feature at $20,000 \text{ km s}^{-1}$, implying the presence of denser material in the cool ejecta. One possible origin for high velocity, dense ejecta is the shell that can form as a result of the diffusion of radiation at the time of shock breakout (Chevalier 1976); if this is the origin, it represents the highest velocity material in the ejecta. We assume that the outer density profile can be approximated as a power law out to this high velocity and take $n = 7$ or 9 . The value of A is equivalent to specifying the density in the ejecta at some particular velocity and age. The model of Baron et al. (2000) for 1999 Oct 29 has $\rho_{sn} = 0.4 \times 10^{-20} \text{ g cm}^{-3}$ at $10,000 \text{ km s}^{-1}$ at an age of 1 year. This value is in approximate accord with the density found in models with a broken power law density profile, mass of 10 M_\odot , and energy of $1 \times 10^{51} \text{ ergs}$ (Chevalier & Fransson 1994).

The density in the wind is $\rho_w = \dot{M}/(4\pi r^2 v_w)$, where \dot{M} is the mass loss rate and v_w is the wind velocity. We take $\dot{M}_{-6} = \dot{M}/10^{-6} \text{ M}_\odot \text{ yr}^{-1}$ and $v_{w1} = v_w/10 \text{ km s}^{-1}$ as reference values. The interaction of the supernova with a freely expanding wind leads to a shocked shell with radius $R \propto t^{0.8}(n = 7)$ or $t^{6/7}(n = 9)$. This shell is the source of the X-ray emission. The low observed X-ray luminosity suggests that the shocked gas is not radiative; this can be checked for consistency after a model is produced. Under these conditions, the X-ray luminosity is expected to be dominated by emission from the reverse shock region, which is relatively cool, as observed. The luminosity of the shell can be estimated from eq. (3.10) of FLC96

$$L_{rev} = 2.0 \times 10^{35} \zeta(n-3)(n-4)^2 T_8^{-0.24} e^{-0.116/T_8} \left(\frac{\dot{M}_{-6}}{v_{w1}} \right)^2 V_4^{-1} \left(\frac{t}{10 \text{ days}} \right)^{-1} \text{ ergs s}^{-1} \text{ keV}^{-1}, \quad (2)$$

where ζ is 0.86 for solar abundances and 0.60 for $n(\text{He})/n(\text{H}) = 1$, $T_8 = T/10^8 \text{ K}$, and V_4 is the peak velocity in units of 10^4 km s^{-1} . Baron et al. (2000) find possible evidence for enhanced

He in SN 1999em, but this is uncertain and is probably not expected in a Type II-P supernova. We take $\zeta = 0.86$; the uncertainty is small. On 1999 Nov 1, which we take to be day 4, the observed luminosity is 2×10^{38} erg s $^{-1}$ and the temperature is 5.0 keV. With $V_4 = 1.5$, we find that $\dot{M}_{-6}/v_{w1} \approx 1$ ($n = 9$) or 2 ($n = 7$), quite similar to the value of $\dot{M}_{-6}/v_{w1} \sim 2$ obtained above from the radio observations. With this mass loss rate, the cooling time for the gas, as deduced from eq. (3.7) of FLC96, is 31 days for $n = 9$ and is longer for the $n = 7$ case, which justifies our use of the adiabatic expression for the X-ray luminosity. The cooling time grows more rapidly than the age, so we expect non-radiative evolution through the time of our observations. If cooling were important, a dense shell would form that could absorb X-ray emission from the reverse shock wave, as appeared to occur in the initial evolution of SN 1993J (FLC96; Suzuki & Nomoto 1995). Reradiation of the absorbed emission can give broad optical emission lines, as observed in SN 1993J at ages $\gtrsim 1$ year. Such lines were not observed in SN 1999em, which is consistent with non-radiative evolution.

From eq. (2.2) of FLC96 with $n = 9$, we find that the maximum velocity for $n = 9$ is

$$V = \left(\frac{4\pi\rho_o t_o^3 v_o^9 v_w}{15\dot{M}} \right)^{1/7} t^{-1/7}, \quad (3)$$

where ρ_o specifies an ejecta density at a particular time t_o and velocity v_o , as described above. At $t = 4$ days with $\rho_o = 0.4 \times 10^{-20}$ g cm $^{-3}$ at $v_o = 10,000$ km s $^{-1}$ and $t_o = 1$ year and $\dot{M}_{-6}/v_{w1} = 1$, we have $V = 13,000$ km s $^{-1}$. For the $n = 7$ case with $\dot{M}_{-6}/v_{w1} = 2$, we have $V = 14,000$ km s $^{-1}$ and $V \propto t^{-0.2}$. These velocities are lower than the highest velocities deduced by Baron et al. (2000) on 1999 Oct 29 (day 1), but there is some uncertainty in the high velocity and there may have been rapid evolution at early times.

The shock velocity determines the temperature of the reverse shock region. From eqs. (3.1) and (3.2) of FLC96, we have $T_{\text{rev}} = 2.4V_4^2$ keV for $n = 9$, so that with $V_4 = 1.3$, $T_{\text{rev}} = 4.1$ keV. For $n = 7$ with $V_4 = 1.4$, we have $T_{\text{rev}} = 9.2$ keV. The observed temperature on 1999 Nov 1 falls between these two cases. The predicted evolution of the temperature is $T \propto V^2 \propto t^{-2/(n-2)} \propto t^{-2/7}$ ($n = 9$) and $\propto t^{-0.4}$ ($n = 7$). Table 3 compares this predicted evolution with that observed. The observations show a clear cooling, as expected. An additional factor could be the lack of electron-ion equilibration at the reverse shock front; if it is not achieved, the electrons are cooler than the above estimate. From eq. (3.6) of FLC96, the expected conditions are such that the equilibration timescale is comparable to the age throughout the evolution, so that no firm conclusion can be drawn. The fact that cooling of the emission is clearly observed argues for a relatively flat density profile for the ejecta, as also found by Baron et al. (2000) from optical spectroscopy.

An estimate of the expected evolution of the total X-ray luminosity, L_x , is given by Chevalier & Fransson (1994). When free-free emission dominates ($T \geq 4 \times 10^7$ K), $L_x \propto t^{-1}$, and when lines dominate ($10^5 \leq T < 4 \times 10^7$ K), $L_x \propto t^{-0.69}$ ($n = 9$) or $\propto t^{-0.56}$ ($n = 7$). The observed evolution is less steep than t^{-1} and is closer to the expectation for line emission. The observed temperatures indicate that there should be a transition between these cases. Again, the observations are in

approximate accord with expectations.

One aspect of the X-ray observations that is not compatible with the simplest wind interaction model is the increase of the soft X-ray flux on 2000 Feb 2 (day 102, see Fig. 2). In our model, the emission is primarily from the shocked ejecta, so the increase could be due to a region of increased density in the ejecta. At this age, the velocity of the ejecta entering the reverse shock front is $\sim 8,000 \text{ km s}^{-1}$. Alternatively, the emission could be from an inhomogeneity in the circumstellar wind. The smooth wind is shocked to a temperature $\sim 10^9 \text{ K}$, so that a density contrast of ~ 100 is needed for the inhomogeneity. The inhomogeneity must be large to affect the total luminosity, but a substantial change in stellar mass loss characteristics at only 10^{16} cm from the star is unlikely. The fact that the change is transitory also argues against a change in mass loss properties at this point.

Although SN 1999em was detected as a radio source, the radio light curves are not well defined because of the low radio flux density. The early observations were not of sufficient sensitivity to detect the source so the time of light curve peak and the early absorption process are not well defined. The 8.44 GHz observations are the most useful in this regard. The observed flux evolution of other radio supernovae is $\propto t^{-0.7}$, or steeper (Weiler et al. 1986), at late times so that the 8.44 GHz upper limit on day 7 probably indicates that absorption was significant at that time. With this value for the time of peak flux at 8.44 GHz (actually a lower limit), we can place SN 1999em on a diagram of peak radio luminosity vs. time of peak (Fig. 6). The diagonal lines show the velocity of the shocked shell if synchrotron self-absorption were the important process for the early absorption (Chevalier 1998). The position of SN 1999em gives about $10,000 \text{ km s}^{-1}$, or less, as the shell velocity. Thus, it is just possible that synchrotron self-absorption was important at early times but more likely that another process, probably free-free absorption by the unshocked wind, was dominant. From eq. (2.3) of FLC96, the 8.44 GHz free-free optical depth on day 7 with V_4 and \dot{M}_{-6}/v_{w1} as deduced above is $\tau = 0.2T_5^{-3/2}$ ($n = 9$) or $0.5T_5^{-3/2}$ ($n = 7$), where T_5 is the temperature of the unshocked wind in units of 10^5 K . The $n = 7$ case is somewhat more consistent with the observations because of the higher mass loss rate deduced for this case.

The free-free absorption of the radio emission depends on the circumstellar temperature. Eastman et al. (1994) find from a simulation of a Type II-P explosion an effective temperature at out-break of $T_{\text{eff}} = 1.8 \times 10^5 \text{ K}$ and luminosity $9 \times 10^{44} \text{ erg s}^{-1}$. This temperature is similar to that used in one model by Lundqvist & Fransson (1991) for SN 1987A (their Table 1). Their model with $\dot{M}_{-6}/v_{w1} = 0.4$ gives a wind temperature of $1.2 \times 10^5 \text{ K}$ for $T_{\text{eff}} = 2 \times 10^5 \text{ K}$. Because of the low wind density, this temperature is not sensitive to the mass loss rate and is mainly set by the outburst radiation temperature. An approximate temperature in the wind of SN 1999em should therefore be $T_5 \approx 1.2$. The temperature at ~ 30 days should not be very different because of the low wind density. X-ray heating by the shock has not been included here, but is probably not important because of the low X-ray luminosity.

Overall, the X-ray and radio observations of SN 1999em are consistent with the non-radiative

interaction of supernova ejecta with a power law profile ($n \sim 7$) interacting with a pre-supernova wind with $\dot{M}_{-6}/v_{w1} \approx 2$. We estimate the accuracy of this mass loss density to be a factor of 2. The X-ray emission is primarily from the shocked ejecta and the model can account for the luminosity, temperature, and temperature evolution of the emission. It does not account for the large soft X-ray flux observed on day 102. The radio observations are compatible with this general picture and suggest a comparable mass loss rate.

5.2. SN 1998S

The high X-ray luminosity of SN 1998S places it in the same class as the X-ray bright Type IIn supernovae SNe 1978K, 1986J, 1988Z, and 1995N. Fox et al. (2000) discussed X-ray observations of SN 1995N and summarized the results on the other supernovae. SN 1998S is at the low end of the X-ray luminosities spanned by these sources; SN 1995N had an X-ray luminosity of 1.5×10^{41} erg s $^{-1}$ at an age of 2.0 years.

The optical emission from SN 1998S shows both narrow and broad lines that can be attributed to circumstellar interaction (Fassia et al. 2000; Leonard et al. 2000). The narrow lines are presumably from dense circumstellar gas that is heated and ionized by the supernova radiation. Although high velocities ($V_4 \approx 1$) are observed in the early evolution of SN 1998S, by day 494 the maximum observed velocities were $V_4 = 0.5 - 0.6$ (Leonard et al. 2000). These velocities are much higher than the estimated velocity of gas at the photosphere, indicating that the emission is from circumstellar interaction.

The interpretation of the X-ray emission from Type IIn supernovae is not straightforward because of the possibility that the emission is from shocked circumstellar clumps (see, e.g., Weiler et al. 1990 and Chugai 1993 on SN 1986J and Van Dyk et al. 1993 on SN 1988Z). The radio results for SN 1998S indicate that the CSM is likely clumpy or filamentary (Lacey et al. 2001). However, if our finding of an overabundance of Fe is correct, the X-ray emission is expected to be from shocked supernova ejecta. If the interaction can be approximately described by smooth ejecta running into a smooth circumstellar wind, the temperature behind the reverse shock front is $T_{\text{rev}} = 2.4V_4^2$ keV ($n = 9$), $5.4V_4^2$ keV ($n = 7$), or $9.6V_4^2$ keV ($n = 6$). It is difficult to produce the high observed temperature ($T \approx 10$ keV) unless there is unseen high velocity gas and the ejecta density profile is relatively flat. The observations do not show the cooling that is expected as the shock interaction region decelerates, but the range in time is not large enough for the effect to clearly show up.

The X-ray luminosity shows a clear decline with time, approximately $\propto t^{-1.3}$. This is approximately what is expected for free-free emission from a non-radiative shock region (t^{-1} dependence as discussed above), so we can again use eq. (2) to estimate the mass loss rate. The result is $\dot{M}_{-4}/v_{w1} = (1 - 2)$, where $\dot{M}_{-4} = \dot{M}/10^{-4} M_{\odot} \text{ yr}^{-1}$, if $n = 6$ and $V_4 = 1$ on day 665, again comparable to that determined from radio modeling of $\dot{M}_{-4}/v_{w1} \sim 2$. A high mass loss rate is required to produce the X-ray luminosity, but the cooling time is still longer than the age. The

assumption of a non-radiative reverse shock region is justified. In this model, the X-ray luminosity of the forward shock region is comparable to that from the reverse shock. However, the higher temperature of the forward shock region implies that the reverse shock dominates the emission in the energy band that we observed.

The radio luminosity of SN 1998S is low for a radio supernova with a late turn-on time (see Fig. 6). This implies that synchrotron self-absorption was not important for the early absorption.

This model for SN 1998S can account for the basic features of the X-rays. The flat supernova density profile implies that much of the supernova energy is in high velocity ejecta. A similar deduction was made by Chugai & Danziger (1994) for SN 1988Z. The possible Fe overabundance requires that some Fe be mixed out to a high velocity in the ejecta. The finding that X-ray emitting Fe-rich gas is present at high velocity in Cas A (Hughes et al. 2000) shows that this can occur in supernovae. In theoretical models of aspherical explosions, Fe-rich matter is naturally ejected at high velocities, which well explains the peculiar late spectral features of SN 1998bw (Maeda et al. 2000). The polarization and spectral line profiles observed in SN 1998S (Leonard et al. 2000) show that the explosion was complex and that the spherically symmetric model described here must be an oversimplification.

6. Summary

Observations at radio, optical, and X-ray wavelengths have allowed the estimation of the physical parameters of two quite different Type II SN examples, Type II-P SN 1999em and Type IIn SN 1998S. From these results it is possible to study, over a broad wavelength range, the physical parameters of the explosions and the structure and density of the pre-SN stellar wind established CSMs. Such results are of importance for estimation of the properties of the pre-SN star and its last stages of evolution before explosion (e.g., Nomoto, Iwamoto, & Suzuki 1995). However, because of the great diversity of Type II (and related Type Ib/c) SNe, only the multiwavelength study of additional examples can yield a comprehensive understanding of the last stages of massive star evolution.

7. Acknowledgments

DP acknowledges that this material is based upon work supported under a National Science Foundation Graduate Fellowship. WHGL and RAC gratefully acknowledge support from NASA. RAC is grateful to E. Baron for useful correspondence. KWW wishes to thank the Office of Naval Research (ONR) for the 6.1 funding supporting this research. Additional information and data on radio emission from SNe can be found on <http://rsd-www.nrl.navy.mil/7214/weiler/> and linked pages. KN has been supported in part by the Grant-in-Aid for COE Scientific Research (07CE2002, 12640233) of the Ministry of Education, Science, Culture, and Sports in Japan.

REFERENCES

Anders, E., & Grevesse, N., 1989, *Geochim. Cosmochim. Acta*, 53, 197

Arnaud, K., 1996, in Jacoby, G., & Branes, J., eds, *ASP Conf. Ser. Vol. 101, Astronomical Data Analysis Software and Systems V*, Astron. Soc. Pac., San Francisco

Baron, E., Branch, D., Hauschildt, P. H., Filippenko, A. V., Kirshner, R. P., Challis, P. M., Jha, S., Chevalier, R. A., Fransson, C., Lundqvist, P., Garnavich, P., Leibundgut, B., McCray, R., Michael, E., Panagia, N., Phillips, M. M., Pun, C. S. J., Schmidt, B., Sonneborn, G., Suntzeff, N. B., Wang, L., & Wheeler, J. C., 2000, *ApJ*, 545, 444

Bloom, J. S., Kulkarni, S. R., Djorgovski, S. G., Eichelberger, A. C., Cote, P., Blakeslee, J. P., Odewahn, S. C., Harrison, F. A., Frail, D. A., Filippenko, A. V., Leonard, D. C., Riess, A. G., Spinrad, H., Stern, D., Bunker, A., Dey, A., Grossan, B., Perlmutter, S., Knop, R. A., Hook, I. M., & Feroci, M., 1999, *Nature*, 401, 453

Branch, D., Falk, S. W., McCall, M. L., Rybski, P., Uomoto, A. K., & Wills, B. J., 1981, *ApJ*, 244, 780

Canizares, C. R., Kriss, G. A., & Feigelson, E. D., 1982, *ApJ*, 253, L17

Cash, W., 1979, *ApJ*, 228, 939

Chevalier, R. A., 1976, *ApJ*, 207, 872

Chevalier, R. A., 1982, *ApJ*, 259, 302

Chevalier, R. A., & Fransson, C., 1994, *ApJ*, 420, 268

Chevalier, R. A., 1998, *ApJ*, 499, 810

Chugai, N. N., 1993, *ApJ*, 414, L101

Chugai, N. N., & Danziger, I. J., 1994, *MNRAS*, 268, 173

Cohen, M. H., 1996, *The LRIS Polarimeter (Keck Obs. Instrument Manual)*, <http://www2.keck.hawaii.edu:3636/>

Eastman, R. G., Woosley, S. E., Weaver, T. A., & Pinto, P. A., 1994, *ApJ*, 430, 300

Fassia, A., Meikle, W. P. S., Vacca, W. D., Kemp, S. N., Walton, N. A., Pollacco, D. L., Smartt, S., Oscoz, A., Aragón-Salamanca, A., Bennett, S., Hawarden, T. G., Alonso, A., Alcalde, D., Pedrosa, A., Telting, J., Arevalo, M. J., Deeg, H. J., Garzón, F., Gómez-Roldán, A., Gómez, G., Gutiérrez, C., López, S., Rozas, M., Serra-Ricart, M., & Zapatero-Osorio, M. R., 2000, *MNRAS*, 318, 1093

Fesen, R. A., & Becker, R. H., 1990, *ApJ*, 351, 437

Fesen, R. A., & Matonick, D. M., 1993, ApJ, 407, 110

Filippenko, A. V., & Barth, A. J., 1997, IAU Circ. 6794

Filippenko, A. V., 1997, ARA&A, 35, 309

Filippenko, A. V., & Moran, E. C., 1998, IAU Circ. 6830

Filippenko, A. V., et al. 2001, in preparation

Fox, D. W., Lewin, W. H. G., Fabian, A., Iwasawa, K., Terlevich, R., Zimmermann, H. U., Aschenbach, B., Weiler, K., Van Dyk, S., Chevalier, R., Rutledge, R., Inoue, H., & Uno, S., 2000, MNRAS, 319, 1154

Fransson, C., Lundqvist, P., & Chevalier, R. A., 1996, ApJ, 461, 993, (FLC96)

Fransson, C., & Björnsson, C.-I., 1998, ApJ, 509, 861

Garnavich, P., Jha, S., & Kirshner, R., 1998a, IAU Circ. 6832

Garnavich, P., Kirshner, R., Challis, P., Koranyi, D., & Culkins, M., 1998b, IAU Circ. 6845

Gehrels, N., 1986, ApJ, 303, 336

Granslo, B. H., Shanklin, J., Carvajal, J., & Hornoch, K., 1998, IAU Circ. 6846

Höflich, P., 1991, A&A, 246, 481

Hughes, J. P., Rakowski, C. E., Burrows, D. N., & Slane, P. O., 2000, ApJ, 528, L109

Immler, S., Pietsch, W., & Aschenbach, B., 1998, A&A, 331, 601

Khokhlov, A. M., Höflich, P. A., Oren, E. S., Wheeler, J. C., Wang, L., & Chtchelkanova, A. Yu., 1999, ApJ, 524, L107

Lacey, C. K., Weiler, K. W., Van Dyk, S. D., Panagia, N., & Sramek, R. A., 2001, in preparation

Leibundgut, B., Kirshner, R. P., Pinto, P. A., Rupen, M. P., Smith, R. C., Gunn, J. E., & Schneider, D. P., 1991, ApJ, 372, 531

Leonard, D. C., Filippenko, A. V., Barth, A. J., & Matheson, T., 2000, ApJ, 536, 239

Leonard, D. C., Filippenko, A. V., Ardila, D. R., & Brotherton, M. S., 2001a, ApJ, in press

Leonard, D. C., et al., 2001b, in preparation

Li, W.-D., Li, C., Filippenko, A. V., & Moran, E. C., 1998, IAU Circ. 6829

Li, W.-D., et al., 1999, IAU Circ. 7294

Li, W. D., et al., 2000, in *Cosmic Explosions*, ed. S. S. Holt & W. W. Zhang, (New York: AIP), p. 103

Liu, Q.-Z., Hu, J.-Y., Hang, H.-R., Qiu, Y.-L., Zhu, Z.-X., & Qiao, Q.-Y., 2000, *A&AS*, 144, 219

Lundqvist, P., & Fransson, C., 1991, *ApJ*, 380, 575

Maeda, K., Nakamura, T., Nomoto, K., Mazzali, P. A., Patat, F., & Hachisu, I., 2000, *ApJ*, submitted (astro-ph/0011003)

Matzner, C. D., & McKee, C. F., 1999, *ApJ*, 510, 379

Mewe, R., Gronenschild, E. H. B. M., & van den Oord, G. H. J., 1985, *A&AS*, 62, 197

Miller, J. S., & Stone, R. P. S., 1993, *Lick Obs. Tech. Rep.* 66

Niemela, V. S., Ruiz, M. T., & Phillips, M. M., 1985, *ApJ*, 289, 52

Nomoto, K., Iwamoto, K., & Suzuki, T., 1995, *Phys. Rep.* 256, 173

Oke, J. B., Cohen, J. G., Carr, M., Cromer, J., Dingizian, A., Harris, F. H., Labrecque, S., Lucinio, R., Schaal, W., Epps, H., & Miller, J., 1995, *PASP*, 107, 375

Panagia, N., Vettolani, G., Boksenberg, A., Ciatti, F., Ortolani, S., Rafanelli, P., Rosino, L., Gordon, C., Reimers, D., Hempe, K., Benvenuti, P., Clavel, J., Heck, A., Penston, M. V., Macchietto, F., Stickland, D. J., Bergeron, J., Tarenghi, M., Marano, B., Palumbo, G. G. C., Parmar, A. N., Pollard, G. S. W., Sanford, P. W., Sargent, W. L. W., Sramek, R. A., Weiler, K. W., & Matzik, P., 1980, *MNRAS*, 192, 861

Patat, F., Barbon, R., Cappellaro, E., & Turatto, M., 1993, *A&A*, 98, 443

Patat, F., Barbon, R., Cappellaro, E., & Turatto, M., 1994, *A&A*, 282, 731

Predehl, P., & Schmitt, J. H. M. M., *A&A*, 293, 889

Schlegel, E., 1990, *MNRAS*, 244, 269

Sohn, Y.-J., & Davidge, T. J., 1998, *AJ*, 115, 130

Sollerman, J., Cumming, R. J., & Lundqvist, P., 1998, *ApJ*, 493, 933

Suzuki, T., & Nomoto, K., 1995, *ApJ*, 455, 658

Tully R.B., 1988, *Nearby Galaxies Catalog*, Cambridge University Press

Van Dyk, S. D., Weiler, K. W., Sramek, R. A., & Panagia, N., 1993, *ApJ*, 419, L69

Van Dyk, S. D., Lacey, C. K., Sramek, R. A., & Weiler, K. W., 1999, *IAU Circ.* 7322

Wang, L., Howell, D. A., Höflich, P., & Wheeler, J. C., 2001, *ApJ*, in press

Weiler, K. W., Sramek, R. A., Panagia, N., van der Hulst, J. M., & Salvati, M., 1986, *ApJ*, 301, 790

Weiler, K. W., Panagia, N., & Sramek, R. A., 1990, *ApJ*, 364, 611

Weiler, K. W., Van Dyk, S. D., Panagia, N., Sramek, R. A., & Discenna, J. L., 1991, *ApJ*, 380, 161

Weiler, K. W., Van Dyk, S. D., Panagia, N., & Sramek, R. A., 1992, *ApJ*, 398, 248

Wheeler, J. C., Yi, I., Höflich, P., & Wang, L., 2000, *ApJ*, 537, 810

Willick, J. A., Courteau, S., Faber, S. M., Burstein, D., Dekel, A., & Strauss, M. A., 1997, *ApJ*, 109, 333

Table 1. *Chandra* Observations of SN 1999em.

Date	Day (From Ref.)	Length (ksec)	Length After Filtering (ksec)	Count Rate (cts ksec ⁻¹)	$F_x[2-10 \text{ keV}]$ / $F_x[0.4-2 \text{ keV}]$
1999 Nov 1	4	29.0	21.6	3.70	2.1 ± 0.9
1999 Nov 13	16	26.0	10.6	2.46	0.8 ± 0.4
1999 Dec 16	49	35.3	35.1	1.02	0.7 ± 0.5
2000 Feb 7	102	38.5	23.9	1.84	0.2 ± 0.1
2000 Oct 30	368	26.4	26.4	0.46	0.9 ± 0.5

Table 2. *Chandra* Observations of SN 1998S.

Date	Day (From Ref.)	Length (ksec)	Length After Filtering (ksec)	Count Rate (cts ksec ⁻¹)
2000 Jan 10	668	18.9	18.9	34.4
2000 Mar 7	725	23.4	23.1	30.3
2000 Aug 1	872	19.8	19.8	25.8
2001 Jan 14	1038	29.2	29.2	19.5

Table 3. X-ray Temperature Evolution of SN 1999em.

Day (From Ref.)	Obs. MEKAL kT (keV)	Obs. Brems. kT (keV)	Model kT ($n = 7$) (keV)	Model kT ($n = 9$) (keV)
4	$5.0^{+5.1}_{-2.1}$	$5.2^{+11.5}_{-2.3}$	9.2	4.1
15	$2.5^{+2.7}_{-0.9}$	$2.3^{+5.9}_{-1.1}$	5.4	2.8
49	$2.9^{+2.6}_{-1.1}$	$2.2^{+3.2}_{-0.9}$	3.4	2.0
102	$0.8^{+0.2}_{-0.1}$	$1.1^{+0.7}_{-0.4}$	2.5	1.6
368	$1.0^{+0.7}_{-0.3}$	$1.5^{+6.5}_{-0.8}$	1.5	1.1

Note. — Listed uncertainties are 90% confidence intervals.

Table 4. VMEKAL Fits to the Spectra of SN 1998S.

Day (From Ref.)	kT (keV)	Fe Abund. (w.r.t. solar)	$\chi^2/\text{d.o.f.}$	$L_{\text{x}}[2\text{--}10 \text{ keV}]^{\text{a}}$ (erg s $^{-1}$)
668	$10.4^{+81.9}_{-2.2}$	$6.5^{+63}_{-6.5}$	82.7/96	9.3×10^{39}
725	$9.6^{+5.5}_{-2.2}$	$4.2^{+7.3}_{-2.6}$	71.7/71	8.8×10^{39}
872	$10.4^{+14.1}_{-4.2}$	$2.8^{+15.8}_{-2.8}$	65.8/75	6.1×10^{39}
1038	$8.0^{+3.7}_{-2.1}$	$5.4^{+14.5}_{-3.5}$	57.0/59	5.3×10^{39}

Note. — Listed uncertainties are 90% confidence intervals.

^afor $z = 0.003$ and $H_0 = 50$

Table 5. Gaussian Fits to the Fe Line of SN 1998S.

Day (From Ref.)	Energy (keV)	FWHM (eV)	Equiv. Width (keV)
668	$6.7^{+0.1}_{-0.1}$	122^{+348}_{-122}	$1.1^{+0.8}_{-0.8}$
725	$6.8^{+0.1}_{-0.1}$	130^{+102}_{-130}	$2.4^{+1.3}_{-1.4}$
872	$6.9^{+0.2}_{-0.3}$	134^{+802}_{-134}	$1.6^{+1.4}_{-1.4}$
1038	$6.7^{+0.4}_{-0.4}$	48^{+1560}_{-48}	$1.0^{+1.0}_{-0.9}$

Note. — Listed uncertainties are 90% confidence intervals.

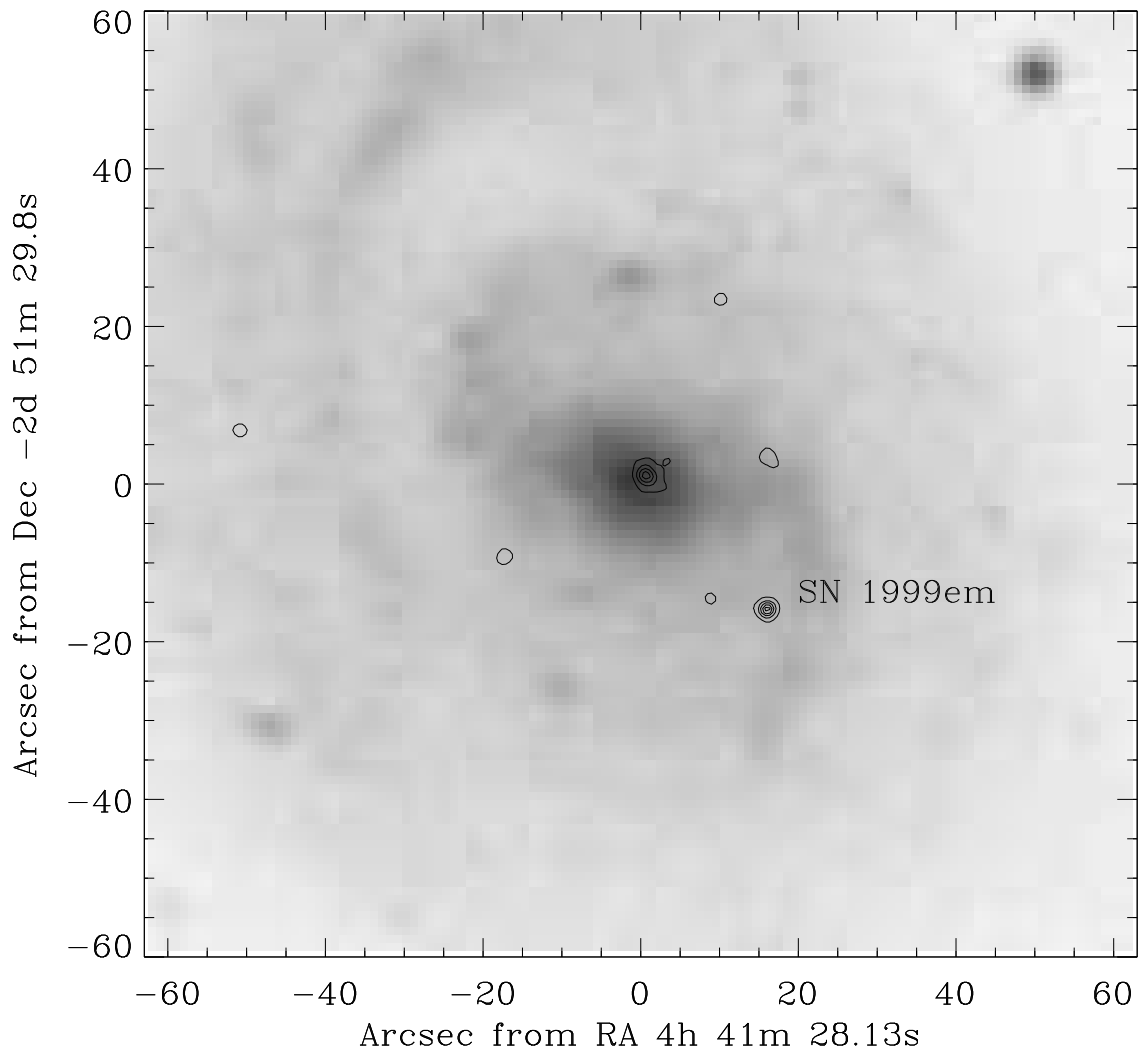


Fig. 1.— NGC 1637 in optical and X-rays. X-ray contours from the first *Chandra* observation of SN 1999em are overlaid on a DSS image of the host galaxy.

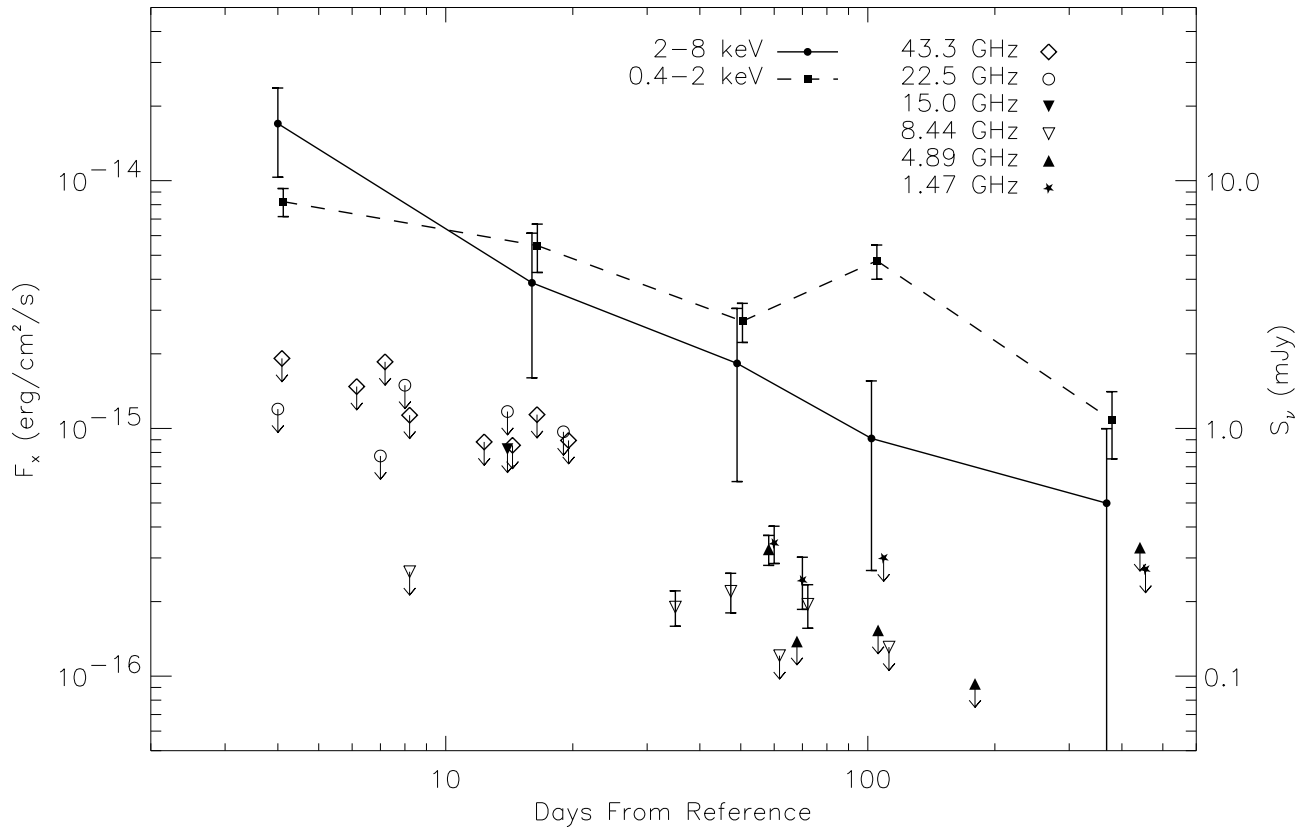


Fig. 2.— X-ray and radio light curves of SN 1999em. The detections are shown with error bars while the upper limits are shown with downward arrows. Radio flux densities are plotted with the appropriate symbols. The absorbed X-ray flux is plotted in both the 2–8 keV (solid line) and 0.4–2 keV (dashed line) bands. The hard X-rays follow a steady decline, but the soft X-rays double from the third observation to the fourth.

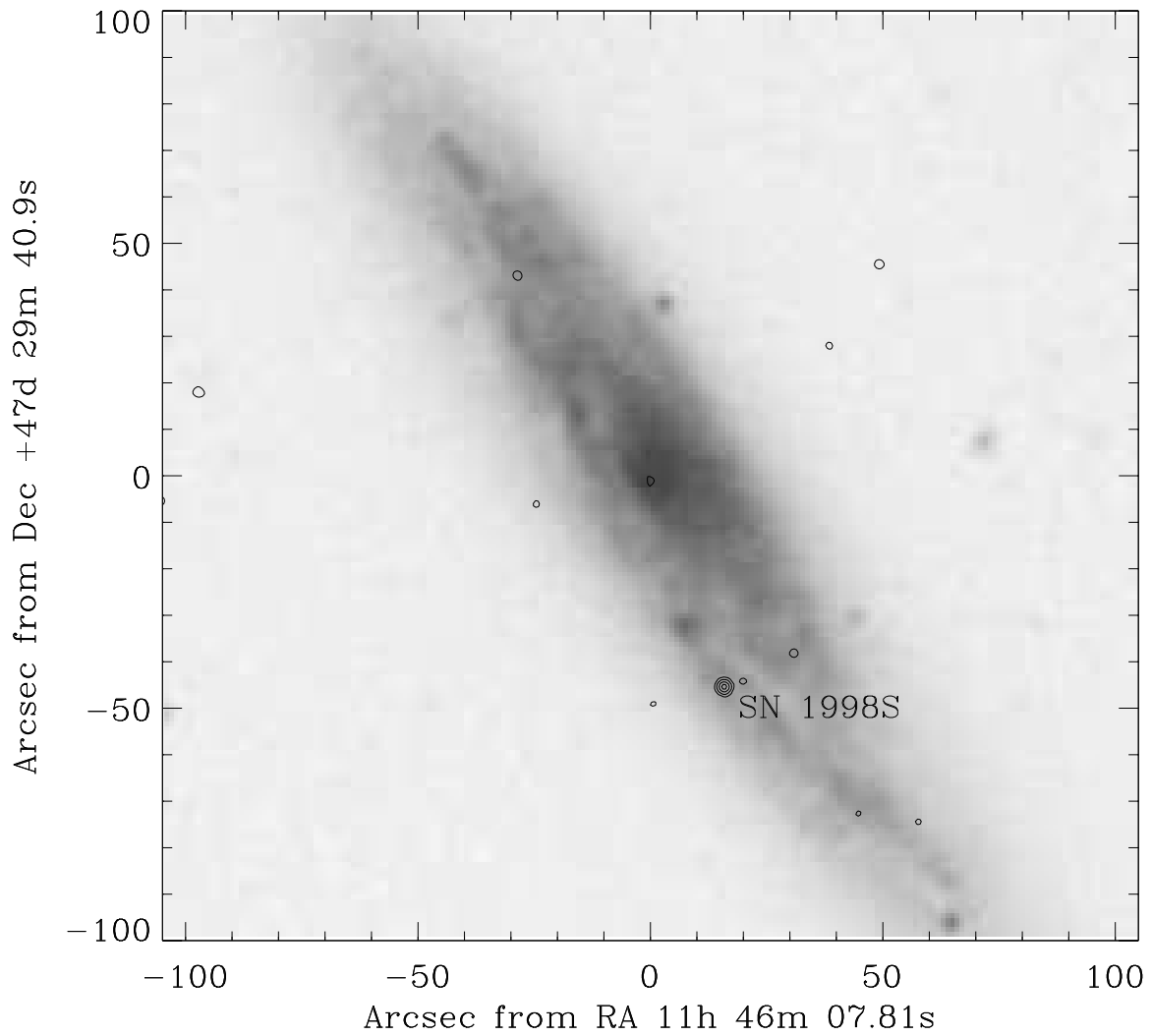


Fig. 3.— NGC 3877 in optical and X-rays. X-ray contours from the first *Chandra* observation of SN 1998S are overlaid on a DSS image of the host galaxy.

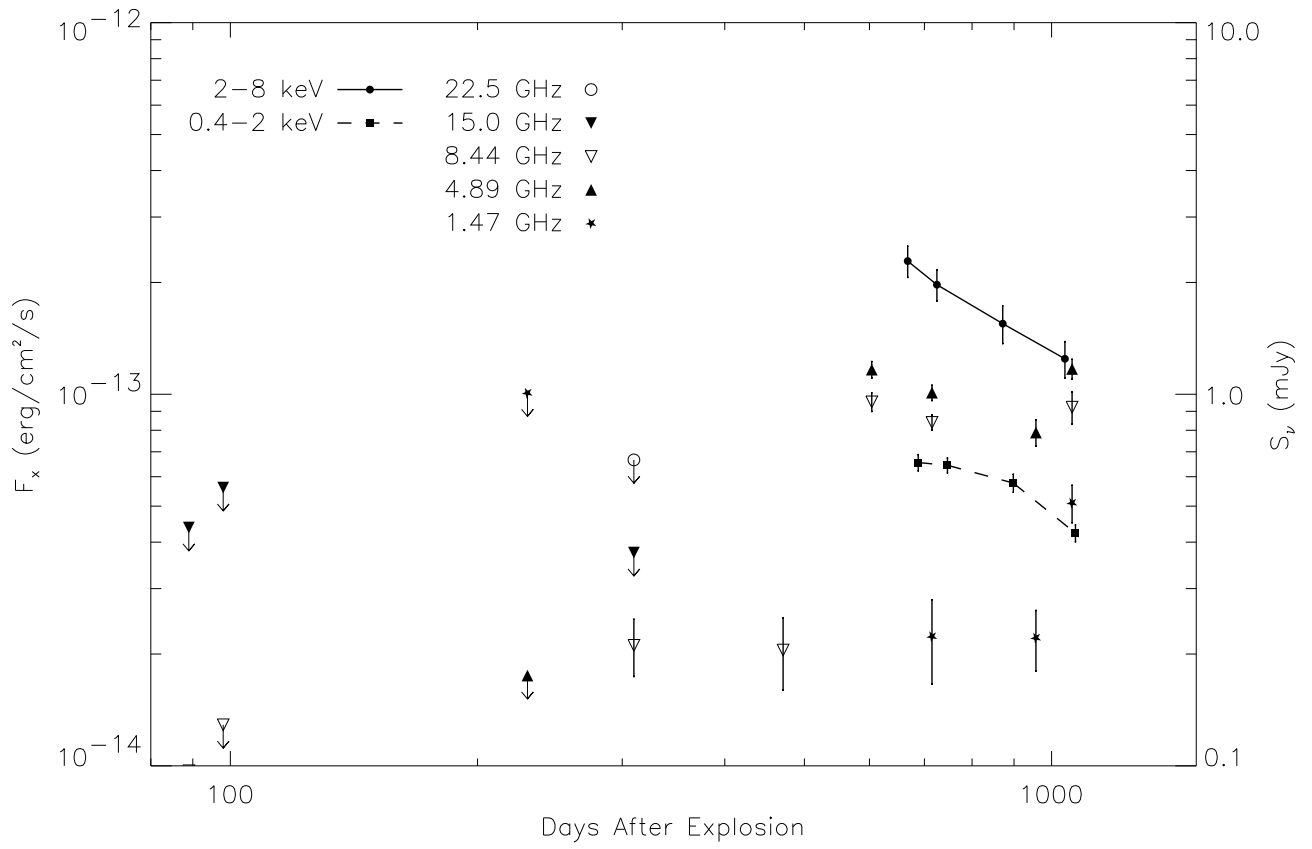


Fig. 4.— X-ray and radio light curves of SN 1998S. The detections are shown with error bars while the upper limits are shown with downward arrows. The absorbed X-ray flux declines in both the hard (solid lines) and soft (dashed lines) bands. Radio flux densities rise at all mid-cm wavelengths.

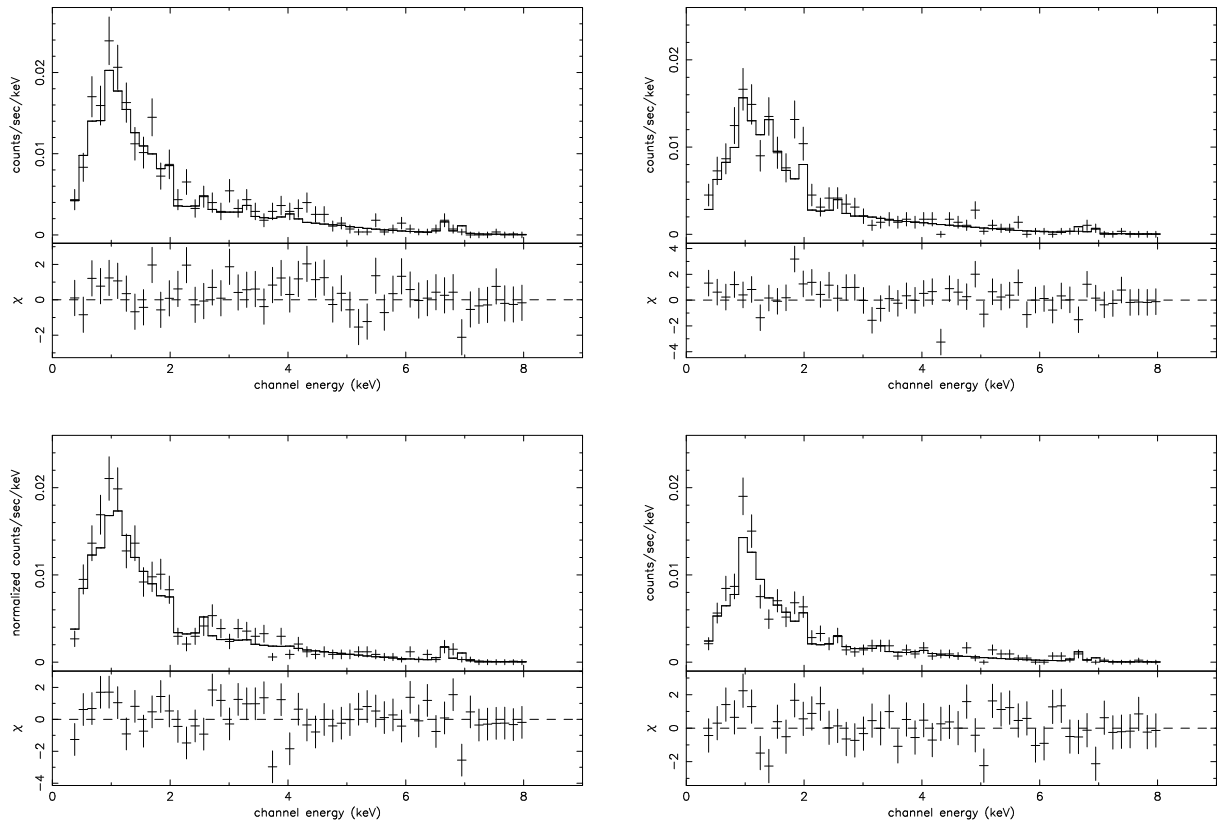


Fig. 5.— Spectra of SN 1998S. The first observation is in the upper left, the second in the lower left, the third in the upper right, and the fourth in the lower right. Best-fit VMEKAL models are overplotted on evenly binned data.

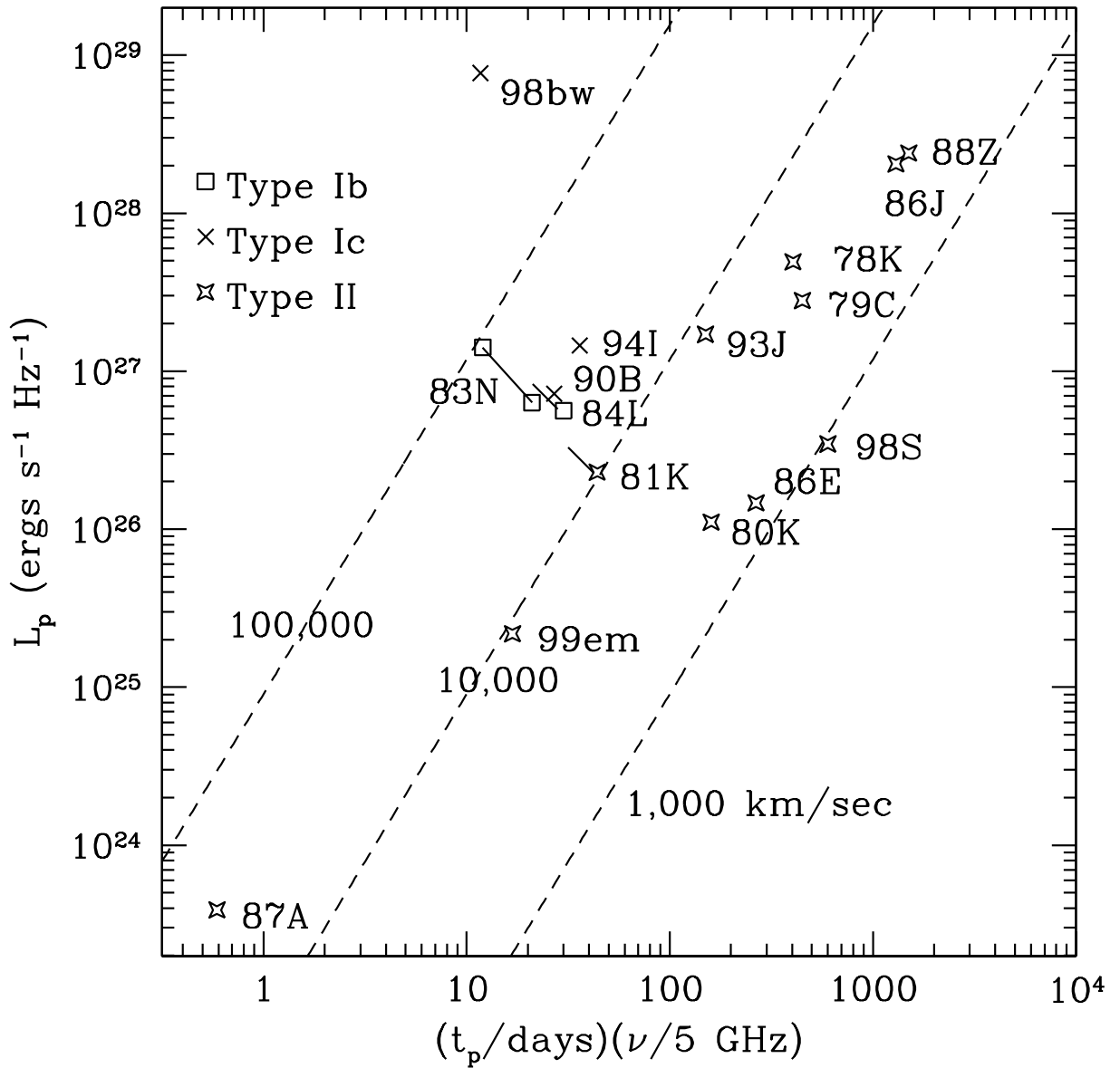


Fig. 6.— The peak spectral radio luminosity vs the product of the time of the peak and the frequency of the measurement, based on Fig. 4 of Chevalier (1998) with the addition of SN 1998bw, SN 1998S, and SN 1999em. The observed supernovae are designated by the last two digits of the year and the letter, and are of Types II (stars), Ib (squares), and Ic (crosses). The dashed lines show the mean velocity of the radio shell if synchrotron self-absorption is responsible for the flux peak; an electron spectrum $N(E) \propto E^{-2.5}$ is assumed.